JOURNAL OF THERMOPHYSICS AND HEAT TRANSFER
Vol. 23, No. 2, April–June 2009

Shock Radiation Measurements for Mars Aerocapture Radiative Heating Analysis

Jay H. Grinstead* and Michael J. Wright†
NASA Ames Research Center, Moffett Field, California 94035
and
David W. Bogdanoff† and Gary A. Allen‡
ELORET Corporation, Moffett Field, California 94035

DOI: 10.2514/1.37281

NASA's In-Space Propulsion Technology program is supporting the development of shock radiation transport models for aerocapture missions to Mars and Venus. Phenomenological models of nonequilibrium shock radiation will be incorporated into high-fidelity flowfield computations used to predict the aerothermal environments for a Mars or Venus aerocapture entry vehicle. These models are validated with shock radiance measurements obtained at flight-relevant conditions. A comprehensive test series in the NASA Ames Electric Arc Shock Tube facility at a representative freestream condition was recently completed. The facility's optical instrumentation enabled spectral measurements of shocked gas radiation from the vacuum ultraviolet to the near infrared. The instrumentation captured the nonequilibrium postshock excitation and relaxation dynamics of dispersed spectral features. A description of the shock tube facility, optical instrumentation, and examples of the test data are presented.

I. Introduction

AEROCAPTURE has been studied extensively as an alternative means of orbital insertion of exploration spacecraft for Mars missions [1]. More recently, a NASA systems study was performed to examine the relative advantages of aerocapture for Venus orbiter and entry missions [2]. In each case, it was found that significant gains in payload mass are possible by obviating the need for the spacecraft to carry chemical propulsion used for deceleration to secure orbit capture. The mission design challenge shifts to the vehicle aeroshell, which protects the spacecraft during the pass through the atmosphere, to realize the required deceleration. Accurate aerothermal environments are needed to select and size the thermal protection system for the vehicle aeroshell. Central to the effort of environment definition is the use of high-fidelity computational fluid dynamics (CFD) simulation. The CFD flow solvers incorporate real-gas energy transport models and have been developed to simulate the aerothermal environments for Earth and planetary atmospheric entry vehicles. The energy transport models, in turn, are developed and validated with relevant ground- and/or flight-test data. At high-enough entry velocities, the energy emitted from shock layer radiation will become a significant part of the total heat flux to the entry vehicle. The high-fidelity radiation transport codes will also rely on physical models that are validated with test data.

The atmosphere of both Mars and Venus consists of about 96% CO_2, 4% N_2, and a trace amount of Ar by volume. When this gas mixture is shocked, several potentially strong radiators are formed, including CO, CN, and carbon atoms. Predictions of the radiative heating generated by these species indicate that shock layer radiation will become significant at velocities above about 7.5 km/s. Radiation has not been a design concern for previous Mars missions due to a combination of low entry velocities and small entry vehicle sizes. For example, the Mars Pathfinder probe (1997) was the fastest Mars entry to date, but was predicted to encounter a maximum of only about 10 W/cm^2 of radiative heating [3] due to its small size. The much-larger Mars Science Laboratory, scheduled for launch in 2011, will encounter only about 0.01 W/cm^2 of radiative heating due to its comparatively low entry velocity. Future Mars aerocapture systems, particularly those in support of crewed missions, will be larger and likely enter at higher velocities. Shock layer radiation will thus be a dominant portion of the entry heating environment for this mission class. For Venus missions, the orbital mechanics of the transfer dictate entry velocities on the order of 11 km/s. At this speed, radiation will be a dominant portion of the total entry heat flux and heat load, even for small entry probes. For example, the Pioneer Venus mission consisted of four entry probes with varying destinations and entry flight path angles. The peak radiative heat flux for these vehicles was predicted to range from 1300 to 3400 W/cm^2 [4], or about half of the total heat flux.

Shortcomings in the current state of shock layer radiation prediction capability for Mars and Venus entries has encouraged the NASA In-Space Propulsion (ISP) Technology program to obtain shock radiance data for the validation of phenomenological models of nonequilibrium radiation transport. To support this effort, shock layer radiation at relevant aerocapture conditions has been investigated experimentally in the NASA Ames Electric Arc Shock Tube (EAST) facility. The EAST facility has the capability to generate shock-heated gas mixtures at velocities and pressures representative of aerocapture trajectories. The nonequilibrium gas downstream of the moving one-dimensional shock wave in the EAST is a good analogue of the gas behind the stagnation shock on the flight vehicle, missing only the flow divergence term and the boundary layer on the surface of the vehicle. Therefore, measurements of the excitation and emission processes that occur as the postshock mixture relaxes toward equilibrium are a direct source of validation data for the physics-based radiation emission and transport codes that will be applied to flight vehicle design.

The emission spectroscopy instrumentation used for EAST testing, which includes imaging and nonimaging spectrographs, enables measurements of shocked gas radiation spectra over the entire frequency range from the vacuum ultraviolet (VUV) to the near infrared (NIR). The imaging spectrographs, in particular, can capture the nonequilibrium postshock excitation and relaxation

Presented as Paper 1272 at the 46th Aerospace Sciences Meeting, Reno, NV, 7–10 January 2008; received 24 February 2008; accepted for publication 20 October 2008.

*Senior Research Scientist, Reacting Flow Environments Branch, MS 230-2. Senior Member AIAA.
†Senior Research Scientist, Reacting Flow Environments Branch, MS 230-2. Associate Fellow AIAA.
‡Senior Research Scientist, Reacting Flow Environments Branch, MS 230-2.

dynamics of dispersed spectral features from the UV to the NIR. The capabilities of the current EAST emission spectroscopy instrumentation were first demonstrated during a test program to investigate the radiation environment for a proposed aerocapture mission to Titan [5]. Early systems analysis of this mission indicated that the total aeroheating encountered during entry, even at moderate velocities, would be dominated by shock layer radiation. This prediction was based upon the unique composition of Titan's atmosphere, which was estimated to consist of about 97% N_2 and 3% CH_4 by volume. When this composition is shocked, gas-kinetic reactions decompose the methane and produce CN, which radiates strongly in the red and violet portions of the spectrum. However, the radiation analysis tools that predicted these high heating rates were not validated for Titan applications. The resulting uncertainty required the use of conservative (optically thin Boltzmann) models to predict the radiative heating for these early systems studies and prompted support for the EAST facility test program for Titan entry shock radiation measurements.

Data from that test series, obtained at gas compositions, freestream pressures, and shock velocities relevant to Titan aerocapture, were used to build a new finite-rate collisional-radiative model. The new model showed the previous estimates of shock layer radiance were too high by factors of up to five [6]. These predictions greatly increase the attractiveness of aerocapture versus traditional chemical propulsion for future Titan missions because the heating rates and loads are now significantly reduced over previous estimates. This, in turn, reduces the mass of the vehicle's thermal protection system (TPS) and opens up the possibility of still-more-efficient low-density TPS material concepts. Results from the EAST facility were also used to perform a risk assessment of the Huygens probe before its January 2005 entry [7] and, later, to calibrate multiple new collisional-radiative models for CN shock layer radiation prediction [8].

The Titan test data clearly demonstrated the value of the EAST facility for shock layer radiation predictions and high-fidelity model development. The data reported here are the beginnings of a similar model development activity for Mars and Venus entries. More data are being taken now that will improve coverage of velocity, density, and wavelength space over those reported in this paper.

Previous researchers have used shock tubes to investigate shock layer radiation from CO_2 systems [9–13]. More recently, Losev et al [14], Zalogin et al. [15], and Kudryatsev et al. [16] conducted a series of shock tube tests in CO_2–N_2–Ar gas mixtures at velocities between 3 and 4 km/s and pressures from 66 to 660 Pa (0.5–5 torr). These experiments were used by Zalogin et al. to develop a master equation model for CN and make estimates of the collisional excitation and deexcitation rates. These rates were later employed by Bose et al. [6] in their collisional-radiative model for Titan entries and showed good agreement with the EAST data. Unfortunately, all of these shock tube test series were conducted at low velocities and at pressures that were about an order of magnitude higher than the peak heating point on a typical Mars aerocapture vehicle. At these higher pressures, nonequilibrium effects would be much smaller, making validation of a nonequilibrium radiation model appropriate for flight predictions based on these data very difficult. Also, the majority of the data from these tests measured the emission at a single wavelength as a function of time, instead of the total integrated radiative power over a large wavelength range needed to validate and calibrate computational models. Finally, these experiments focused on emission from the CN system and did not obtain quantitative data for the CO (4+) system, which is predicted to be the dominant source of shock layer radiation for Mars and Venus entries at the conditions considered in this work.

II. Test Objectives

The current state of shock layer prediction capability for Mars is roughly equivalent to that for Titan before the systems study. Therefore the ISP program decided to obtain new experimental validation data for shock layer radiation at Mars entry conditions to validate current radiation transport models used in high-fidelity flowfield simulations, or to develop new models if necessary. The test condition was chosen based on preliminary systems analyses for an aerocapture maneuver: 0.1 torr (13.3 Pa) preshock pressure, and 8.5 km/s shock velocity. Figure 1 shows the predicted emission spectrum from the UV to the NIR in units of absolute volumetric spectral radiance ($W/cm^3 \cdot \mu m \cdot sr$) at this condition. Although the CN violet system ($B^2\Sigma^+ - X^2\Sigma^+$), C_2 Swan system ($d^3\Pi_g - a^3\Pi_u$), N_2^+ first negative system ($B^2\Sigma_u^+ - X^2\Sigma_g^+$), and several atomic carbon and oxygen lines are present, the major source of radiant energy is from the CO fourth positive system ($A^1\Pi - X^1\Sigma^+$), which radiates in the VUV portion of the spectrum (wavelengths less than ~190 nm). Measuring shock radiance in the VUV region was of primary importance in the current test series.

As shock passage in a shock tube experiment is a transient event, the instrumentation used to measure shock radiance was designed have adequate spatial and temporal resolution to characterize the shock layer dynamics as the shock wave passes an observation window. The optical instrumentation is described in Sec. III.A. The development and validation of phenomenological models of nonequilibrium radiation require spectrally resolved measurements of absolute radiance behind a shock wave. Therefore, the spectroscopic instruments were calibrated to a reference standard spectral radiance source. Process monitoring and facility performance instrumentation was also incorporated to measure critical test parameters, such as shock velocity and driven gas pressure.

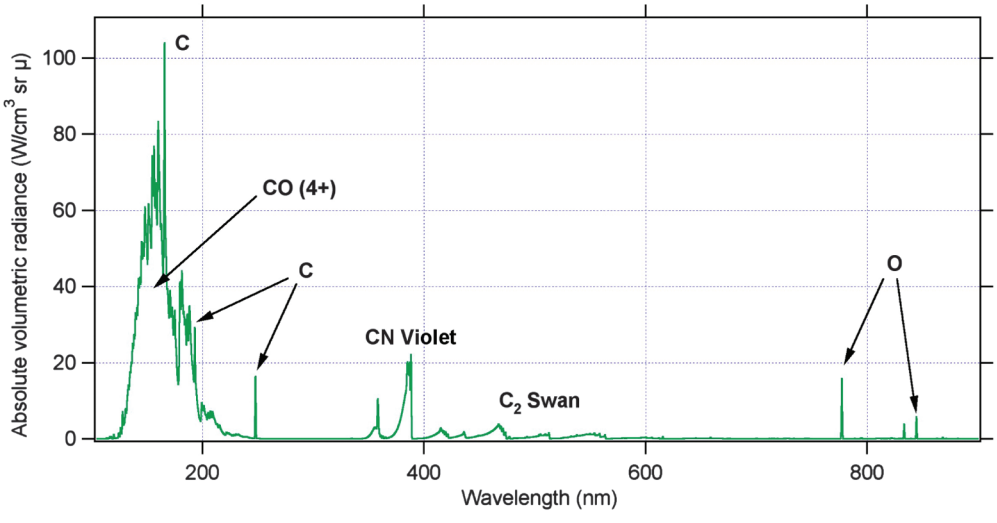

Fig. 1 Predicted emission spectrum of Martian atmosphere at 8.5 km/s and 0.1 torr (13.3 Pa) preshock pressure.

III. Facility Description

The EAST facility at NASA Ames Research Center was developed to simulate high-enthalpy, real-gas phenomena encountered by hypersonic vehicles entering planetary atmospheres. It has the capability of producing superorbital shock speeds using an electric arc driver. The facility was built in the late 1960s to support research in aerothermochemistry of hypervelocity flight through Earth and planetary atmospheres. The use of an electric arc discharge as the driver mechanism permits generation of shock speeds of up to 50 km/s in H_2/He atmospheres. These high shock speeds greatly exceed those achieved with heated light gas, combustion, or free piston drivers. A thorough description of the EAST facility can be found in [17].

A. Instrumentation

The critical instrumentation used in the experiment falls into two categories: emission spectroscopy and facility performance. The spectroscopy instrumentation was designed to measure spectrally resolved shock radiance in absolute units as the shock passes the facility's windows. The shock emission is captured with collection optics that limit the spatial volume viewed by the instrument, followed by spectral resolving instruments that disperse the emission onto single- or multichannel high-speed photodetectors (see Fig. 2).

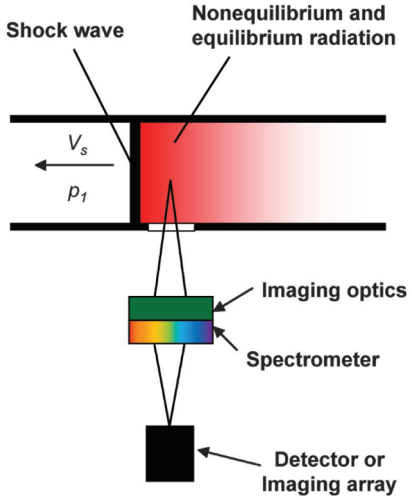

Fig. 2 Emission spectroscopy instrumentation schematic.

The facility performance instrumentation, which consists of high-speed, time-of-arrival pressure transducers and transient digitizers, was used to measure shock arrival times along the driven tube. Shock velocities at the locations of the optical instruments were determined from analysis of the arrival times. Grinstead et al. [18] further described the instrumentation used in this test program.

The capability to capture more than the time-resolved emission of a single spectral feature is realized with an imaging spectrograph. In this configuration, shown schematically in Fig. 3, a monochromator is turned on its side so as to align the entrance slit in a horizontal plane, parallel to the test section axis. The collection optics image an 11 cm region, coincident with the test section axis, through a long, rectangular window in the driven tube wall. The imaged region is focused on the monochromator entrance slit. The monochromator exit slit was removed and replaced by a focal plane array, enabling a segment of the dispersed spectrum to be recorded along one axis of the array. The other axis, aligned parallel to the entrance slit, records the spatial variation of the dispersed spectrum. In this manner, spectra are recorded *simultaneously* at multiple points along the axis of the shock tube.

By using intensified charge-coupled device (CCD) focal plane arrays with short exposure times, the spectral characteristics of the radiating gas behind the shock wave, and a record of how those characteristics change with distance from the shock front, can be captured with high time resolution. The camera is triggered when the shock front nears the downstream end of the rectangular window, and the short exposure time "freezes" the shock image within the field of view of the imaging spectrograph. The shock front and the postshock relaxation zone are recorded at one time instant with multipoint spatial resolution, that is, the two-dimensional image captures, at a single instant, the shock radiance as a function of both wavelength and distance. This approach is complementary to that of Koreeda et al. [19], who used a streak camera coupled to a nonimaging spectrograph to record the temporal variation of shock radiance spectra at a single axial location in a shock tube.

Two 0.3 m monochromators were converted to imaging spectrographs. For each instrument, a spherical mirror and a flat mirror were arranged in a z-shaped configuration (see Fig. 3) to image the axis of the shock tube through a rectangular window and onto the entrance slit. Both instruments imaged the same location through identical windows on opposite sides of the shock tube. Spectrograph 1 was dedicated to measurements from approximately 190 to 500 nm. Spectrograph 2 was dedicated to measurements from approximately 480 to 900 nm. Low- and high-resolution gratings were used to survey wide spectral regions and capture selected atomic and molecular spectral features, respectively.

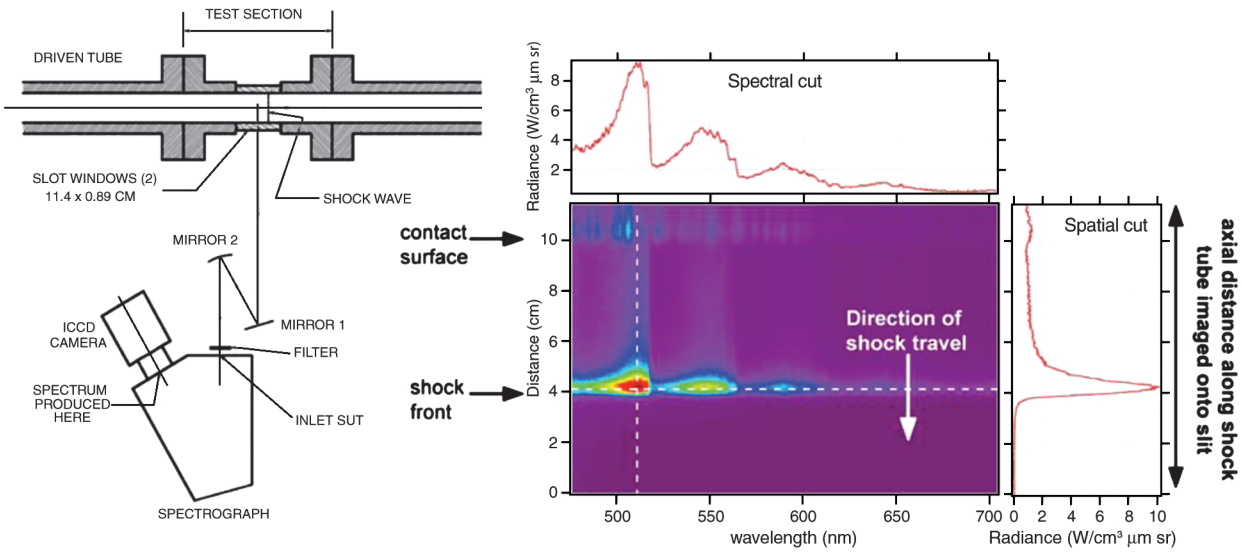

Fig. 3 Shown are the following: a) schematic of one imaging spectrograph configuration, and b) example image of shock radiance at one instant in time showing spectral and spatial cuts. The second imaging spectrograph simultaneously imaged the same region from the opposite side of the shock tube.

The imaging spectrographs were calibrated in wavelength using Hg, Ne, He, and deuterium spectral lamps. The spatial scale was calibrated by imaging a ruled grid placed in the object plane at the shock tube centerline. Calibration of measured signal magnitudes to absolute spectral radiance ($W/cm^2 \cdot \mu m \cdot sr$) was accomplished using tungsten and deuterium reference standard lamps with National Institute of Standards and Technology traceable spectral radiance calibrations. The radiance of a uniform source, such as a reference standard lamp, observed anywhere within the field of view between the shock tube walls is constant, a consequence of the optical (or Lagrange) invariant of the optical system. Because the radiation received by the instruments originates from a volume of gas, however, the radiance values are reported as $W/cm^3 \cdot \mu m \cdot sr$ by normalizing the measured surface spectral radiance ($W/cm^2 \cdot \mu m \cdot sr$) to the driven tube diameter, 10.16 cm. Note that this normalization implicitly assumes that the radiant intensity of the gas is constant across the diameter (i.e., no boundary-layer or curved shock effects). The spectrograph calibration procedure and sample error analyses are documented in [6,20].

An example spectrograph 1 image from the present experiment, calibrated in wavelength, axial distance, and absolute spectral radiance, is shown in Fig. 3b. The arrows mark the location of the shock front and contact surface. The valid test region is defined by these boundaries between the shocked driven gas and the driver gas, respectively. The arrival of the contact surface is indicated by the presence of tungsten and aluminum line radiation; these elements, along with other carbonaceous and fluorinated species, are vaporized by the arc driver and mix with the expanding driver gas. The line plots are spectral and spatial cuts through the image. The locations of these cuts are indicated by the horizontal and vertical dotted lines, respectively. The spectrum at a particular spatial location within the shock layer, in this case, the nonequilibrium peak of the shock front, can be extracted from the image, whereas the spatial variation through the shock layer of a particular spectral feature or wavelength region can also be examined. The use of two imaging spectrographs covering different spectral regions, at the same spatial location, enables analysis of the simultaneous excitation and relaxation dynamics of multiple species and states.

To record emission spectra in the VUV, the optical path from the facility's window through the spectrograph must be evacuated to prevent light absorption by O_2. For this test series, a vacuum-compatible monochromator was converted to a nonimaging spectrograph. A 38-mm-diam, 500-mm-long tube couples a circular window port to the monochromator entrance slit assembly, allowing the entire optical path and the instrument to be kept under vacuum, $<10^{-5}$ torr. Unlike for the imaging spectrographs, there are no imaging optics to convey light from the shock tube to the VUV spectrograph. The entrance slit is aligned perpendicular to the tests section axis. Circular apertures are placed inside the coupling tube to restrict the spatial resolution in the axial direction of the shock tube to approximately 1.3 mm. As with the imaging spectrographs, the monochromator exit slit assembly was removed and replaced by a focal plane array with sensitivity down to 120 nm. Available window materials, however, limited transmission to wavelengths above ~160 nm. The VUV spectrograph provides the same information as the imaging spectrographs, volumetric radiance as a function of wavelength, except there is no multipoint spatial resolution along the shock tube axis. The recorded emission originates from a spatially integrated volume, approximately 1.3 mm in diameter across the 10.16 cm tube. The focal plane array was triggered at the appropriate time to capture the nonequilibrium peak of the shock radiation. As with the imaging spectrographs, signal magnitudes from the VUV spectrograph were calibrated to absolute spectral radiance units using, in this case, a deuterium reference standard lamp.

B. Spectrograph Instrument Configurations and Targeted Spectral Features

The two imaging spectrographs were configured to capture different features of the shock-heated CO_2/N_2 emission at low and high spectral resolution. The center wavelength and span determine the spectral region and extent, respectively, that were recorded for a particular configuration. Table 1 lists the gratings, spectral ranges, camera exposure times, and targeted spectral features for the six configurations used in the test series. The survey, or low-resolution, configurations (1, 2, 4, and 5) overlap each other to ensure continuous coverage from approximately 190 to 880 nm with successive shots at the same nominal test condition. The exposure, or signal-integration, time selected for a particular instrument configuration and test condition represents a compromise between signal-to-noise ratio and time resolution of the measurement; longer exposure times improve the signal-to-noise ratio by collecting more photons but result in spatial smearing of the image due to transit of the gas during the exposure. The amount of smearing can be estimated by considering that a shock wave moving at 8.5 km/s travels 8.5 mm in 1 μs. Higher instrument sensitivities allow for shorter exposure times to reach an acceptable signal-to-noise ratio. The center wavelength, span, and exposure time of the nonimaging VUV spectrograph configuration is also listed in Table 1.

IV. Test Results

The test gas was synthesized to a prescribed composition of 96% CO_2 and 4% N_2 by volume. The preshock pressure was 0.1 torr (13.3 Pa), and the target shock velocity was 8.5 km/s. As noted earlier, these conditions were chosen as representative of the peak radiative heating point on an aerocapture trajectory with an entry velocity of approximately 9 km/s, which is at the high end of trajectories considered for high mass Mars aerocapture missions. Facility variability caused an approximate $\pm 8\%$ deviation from the target shock velocity over the course of the test series; however, the uncertainty in the shock velocity as measured for each run was less than $\pm 1\%$. Figure 4 shows a composite spectrum assembled from two shots at the same nominal condition; two shots were necessary to obtain complete coverage with the four low-resolution spectrograph configurations. Each spectral subregion was extracted from its image at the peak radiance of the shock front, as in Fig. 3. Because of the highly nonlinear dependence of absolute radiance magnitude on shock velocity and the difference of shock velocity between the two shots, the relative radiance values between subregions are not directly comparable. The purpose of the composite spectra is to inspect at a glance the major emission features as labeled in Fig. 4.

The spectral and spatial characteristics of emission from two spectral features were examined in detail to demonstrate the capability of the imaging spectrograph instrumentation to reveal the

Table 1 Spectrograph instrument configurations

Configuration	Spectrograph	Grating density, g/mm	Center wavelngth, nm	Wavelength Span, nm	Spectral resolution, nm	Exposure time range, μs	Features targeted
1	1	246	268	184	0.8	0.25	CO (4+) band system; C lines
2	1	246	386	184	0.8	0.25	CN violet, N_2^+ (1−) band systems
3	1	2400	358	15	0.08	0.5	CN violet 1 − 0 band
4	2	150	590	227	1.7	0.25 − 0.5	C_2 Swan band system
5	2	150	771	227	1.7	0.25 − 0.5	O lines
6	2	1800	558	14	0.1	0.25 − 0.5	C_2 Swan 0 − 1 band
VUV	VUV	150	242	204	1.3	0.5	CO (4+) band system; C lines

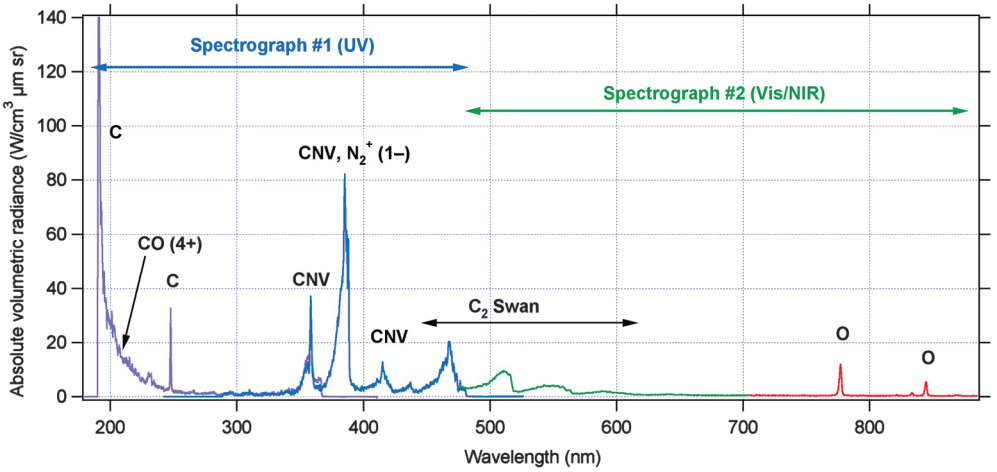

Fig. 4 Composite spectra at nominally 8.5 km/s and 0.1 torr for the Mars atmosphere composition (96%CO_2/4%N_2). The spectrum was assembled from two shots with combinations of the four low-resolution imaging spectrograph configurations. The spectral subregions were extracted from the corresponding images at the shock front (see Fig. 3).

excitation and relaxation dynamics of radiating species. Configuration 3 for spectrograph 1 and configuration 6 for spectrograph 2 (see Table 1) in the UV and NIR, respectively, were used to *simultaneously* capture the $v'(1) - v''(0)$ band of the CN violet system and the $v'(0) - v''(1)$ band of the C_2 Swan system, respectively. The shock velocity was 8.63 ± 0.07 km/s at the 0.1 torr (13.3 Pa) test pressure. Figures 5a and 5b show the spectra of these features extracted from the spectrograph images at the nonequilibrium peak, as in Fig. 3.

The spatial profiles of the radiance of these features through the shock layer were also extracted from the images. Figure 6a shows the profile for a peak of the CN violet $v'(1) - v''(0)$ band at 358.40 nm

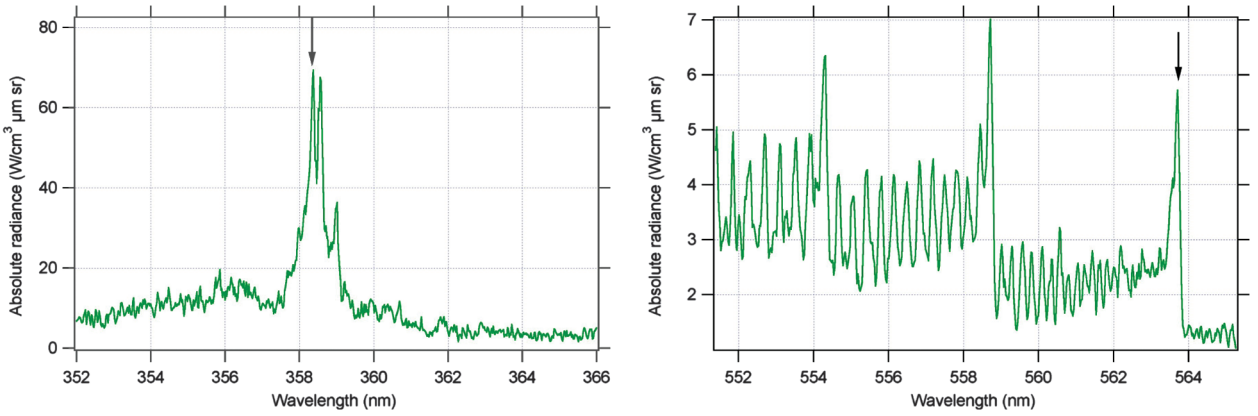

Fig. 5 High resolution spectra obtained simultaneously at 8.63 km/s: a) CN violet $v'(1) - v''(0)$ band (the arrow denotes a peak of the $v'(1) - v''(0)$ band at 358.4 nm), and b) C_2 Swan $v'(0) - v''(1)$ band (the arrow denotes the band head of the $v'(0) - v''(1)$ rotational manifold at 563.7 nm).

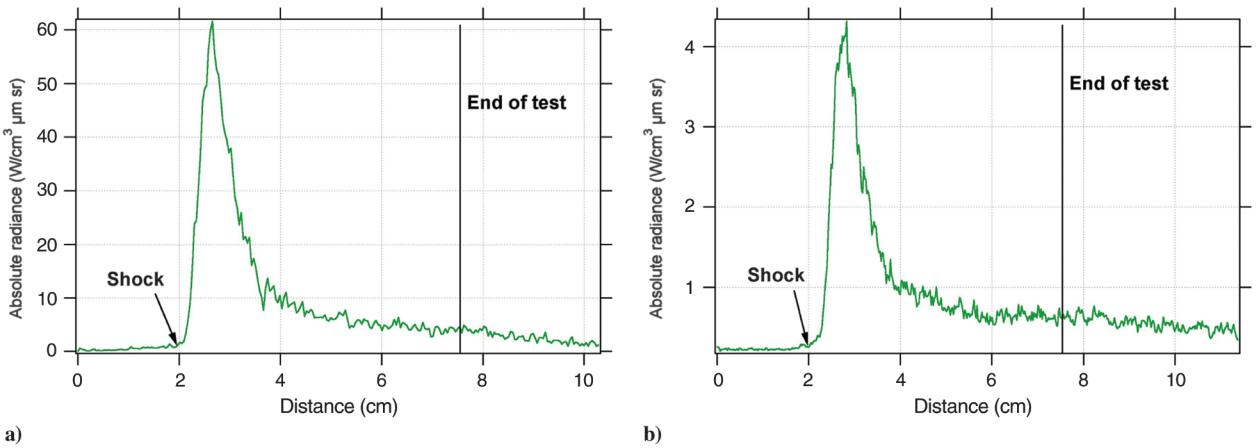

Fig. 6 Spatial variation of radiance through the shock layer at 8.63 km/s for the two features denoted by arrows in Fig. 5: a) peak of the CN violet $v'(1) - v''(0)$ band at 358.40 nm, and b) C_2 Swan $v'(0) - v''(1)$ band head at 563.70 nm. End of test denotes spatial location of driver contact surface.

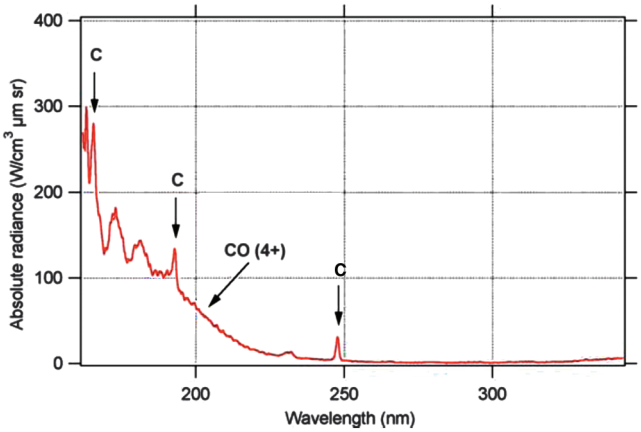

Fig. 7 Vacuum ultraviolet spectrum at 8.65 km/s acquired with the nonimaging VUV spectrograph. The spectrum was captured at the nonequilibrium peak.

(see Fig. 5a) averaged over ±0.07 nm. Figure 6b shows the spatial profile of the C_2 Swan $v'(0) - v''(1)$ band head at 563.70 nm (see Fig. 5b) averaged over ±0.08 nm. The shock wave was traveling from right to left along the spatial scale of the plot, and the spatial location of the shock front coincides with the sharp rise in radiance. The nonequilibrium peak is clearly evident from the profiles. The vertical lines show the locations of the contact surface between the shocked test gas and the driver gas.

Spatial profiles such as these are compared with simulations to discern the kinetic mechanisms governing the population of excited states [6]. The exposure time for the intensified CCD arrays for both spectrographs was 0.5 μs; therefore, the shock moved approximately 4.3 mm during the exposure. As noted in Sec. III.B, the transit of the shock wave during the exposure time smears the recorded spatial profiles of Fig. 6. Before the comparison with the experiment, computed profiles would be convolved with a spatial "boxcar" function to approximate the spatial smear induced by the finite exposure time and shock speed.

The nonimaging VUV spectrograph was also used to capture a portion of the CO (4+) band system down to the transmission limit of the facility's window material (approximately 160 nm). Figure 7 shows this region of the CO (4+) band; additionally, the spectrum shows two atomic carbon lines at 193.1 and 247.9 nm and an atomic carbon multiplet at 165.7 nm. As described earlier, the nonimaging spectrograph collects light at one axial location only; the measurement volume is larger than that of the imaging spectrographs. The detector was triggered as the shock passed the observation window. The nonequilibrium peak of the shock radiation was recorded but without reference to the spatial variation of the excitation and relaxation dynamics enabled by the imaging spectrograph instruments. As predicted in the simulation of Fig. 1, the brightness of the CO (4+) system exceeds that of all other UV–NIR features. To our knowledge, this is the first quantitative spectrograph measurement of the CO (4+) system at relevant conditions for Mars atmospheric entry.

V. Conclusions

Shock radiation testing in the NASA Ames EAST facility was described. The facility has the capability to produce shocked gas conditions for the study of nonequilibrium radiation phenomena encountered by planetary atmospheric entry probes. This test program was designed to address uncertainties in radiation transport models used in Mars aerocapture mission studies. The instrumentation of the EAST facility enabled emission spectroscopy measurements with the spectral and spatial resolution required for analysis of the nonequilibrium shock layer excitation and relaxation kinetics. Selected results from the test series were presented that highlighted the major features of the shock radiation spectrum as well as the capabilities of the emission spectroscopy instrumentation. Future work on radiation model development will make use of these and other data produced from this test series.

Acknowledgments

This work was funded by the NASA In-Space Propulsion program under task agreement M-ISP-03-18 to NASA Ames Research Center. The work of D. Bogdanoff and G. Allen was supported by NASA contract NNA4BC25C to ELORET, Inc. The authors thank D. K. Prabhu for providing computer simulations of the measured spectra, as well as M. Munk and T. Kremic of NASA for their continued support of this work.

References

[1] Vaughn, D., Miller, H. C., Griffin, B., James, B. F., and Munk, M. M., "A Comparative Study of Aerocapture Missions with a Mars Destination," AIAA Paper 2005-4110, July 2005.

[2] Lockwood, M. K., Starr, B. R., Paulson, J. W., Jr., Kontinos, D. A., Chen, Y. K., Laub, B., Olejniczak, J., Wright, M. J., Takashima, N., Justus, C. G., et al., "Systems Analysis for a Venus Aerocapture Mission," NASA TM 2006-214291, March 2006.

[3] Milos, F. S., and Chen, Y.-K., "Mars Pathfinder Entry Temperature Data, Aerothermal Heating, and Heatshield Material Response," *Journal of Spacecraft and Rockets*, Vol. 36, No. 3, 1999, pp. 380–391. doi:10.2514/2.3457

[4] Anon., "Pioneer Venus Large and Small Probe Databook," Bendix Corp. NAS2-830Q, June 1976.

[5] Lockwood, M. K., "Titan Aerocapture System Analysis," AIAA Paper 2003-2799, July 2003.

[6] Bose, D., Wright, M., Bogdanoff, D., Raiche, G. A., and Allen, G. A., "Modeling and Experimental Assessment of CN Radiation Behind a Strong Shock Wave," *Journal of Thermophysics and Heat Transfer*, Vol. 20, 2006, pp. 220–230. doi:10.2514/1.16869

[7] Hollis, B. R., Striepe, S. A., Wright, M. J., Bose, D., Sutton, K., and Takashima, N., "Prediction of the Aerothermodynamic Environment of the Huygens Probe," AIAA Paper 2005-4816, June 2005.

[8] Wright, M. J., Olejniczak, J., Walpot, L., Raynaud, E., Magin, T., Caillaut, L., and Hollis, B. R., "A Code Calibration Study for Huygens Entry Aeroheating," AIAA Paper 2006-0382, Jan. 2006.

[9] Arnold, J. O., Reis, V. H., and Woodward, H. T., "Theoretical and Experimental Studies of Equilibrium and Nonequilibrium Radiation to Bodies Entering Postulated Martian and Venusian Atmospheres at High Speeds," AIAA Paper 65-0166, Jan. 1965.

[10] Thomas, G. M., and Menard, W. A., "Experimental Measurements of Nonequilibrium and Equilibrium Radiation from Planetary Atmospheres," *AIAA Journal*, Vol. 4, No. 2, 1966, pp. 227–237. doi:10.2514/3.3423

[11] Nealy, J. E., and Haggard, K. V., "A Shock Tube Study of Radiation Behind Shock Waves in CO_2 with Application to Venus Entry," *Recent Developments in Shock Tube Research: Proceedings of the 9th International Symposium on Shock Tubes and Waves*, edited by D. Bershader, and W. Griffith, Stanford Univ. Press, Stanford, CA, 1973, pp. 330–339.

[12] Nealy, J. E., "An Experimental Study of Ultraviolet Radiation Behind Incident Normal Shock Waves in CO_2 at Venusian Entry Speeds," AIAA Paper 75-1150, Sept. 1975.

[13] Arnold, J. O., and Nicholls, R. W., "A Shock-Tube Determination of the CN Ground State Dissociation Energy and Electronic Transition Moments for the CN Violet and Red Band Systems," *Recent Developments in Shock Tube Research: Proceedings of the 9th International Symposium on Shock Tubes and Waves*, edited by D. Bershader, and W. Griffith, Stanford Univ. Press, Stanford, CA, 1973, pp. 340–351.

[14] Losev, S. A. Kozlov, P. V., Kuznetsova, L. A., Makarov, V. N., and Romanenko, Y. V., "Radiation of a Mixture CO_2–N_2–Ar in Shock Waves: Experiment and Modeling," *Proceedings of the 3rd European Symposium on Aerothermodynamics for Space Vehicles*, ESA, Paris, 1998.

[15] Zalogin, G., Kozlov, P., Kuznetsova, L., Losev, S., Makarov, V., Romanenko, Y., and Surzhikov, S., "Radiation Excited by Shock Waves in a CO_2–N_2–Ar Mixture: Experiment and Theory," *Technical Physics*, Vol. 46, No. 6, 2001, pp. 654–661. doi:10.1134/1.1379629

[16] Kudryatsev, N. N., Kuznetsova, L. A., and Surzhikov, S. T., "Kinetics and Nonequilibrium Radiation of CO_2–N_2 Waves," AIAA Paper 2001-2728, Jan. 2001.

[17] Sharma, S. P., and Park, C., "Operating Characteristics of a 60-cm and 10-cm Electric Arc Driven Shock Tube, Part I: The Driver; Part II: The Driven Section," *Journal of Thermophysics and Heat Transfer*, Vol. 4, No. 3, 1990, pp. 259–265; 266–272. doi:10.2514/3.175

[18] Grinstead, J. H., Wilder, M. C., Olejniczak, J., Bogdanoff, D. W, Allen, G. A., Dang, K., and Forrest, M. J., "Shock-heated Air Radiation Measurements at Lunar Return Conditions," AIAA Paper 2008-1244, Jan. 2008.

[19] Koreeda, J., Ohama, Y., and Honma, H., "Imaging Spectroscopy of the Nonequilibrium Shock Front Radiation in Air in Shock Waves," *Shock Waves*, Vol. 8, No. 2, 1998, pp. 71–78.doi:10.1007/s001930050100

[20] Grinstead, J. H., Olejniczak, J., Wilder, M. C., Bogdanoff, M. W., Allen, G. A., and Lillard, R., "Shock Heated Air at Lunar Return Conditions: Phase I EAST Test Report," NASA EG-CAP-07-142, 2007.